International Journal of Pharmaceutics: X 9 (2025) 100328

Contents lists available at ScienceDirect

International Journal of Pharmaceutics: X

journal homepage: www.sciencedirect.com/journal/international-journal-of-pharmaceutics-x

Advanced healing potential of simple natural hydrogel loaded with sildenafil in combating infectious wounds

Yifan Lai [a,c,1], Wa Zhang [b,c,1], Yizhang Chen [c,e,f], Jialu Weng [c,e], Yuhan Zeng [c,e,f], Shunfu Wang [a,c], Xiaoying Niu [c], Meilin Yi [c], Haobing Li [c], Xuchen Deng [c], Xiuhua Zhang [a,c,e,f,*], Danyun Jia [d,**], Wenzhang Jin [a,b,c,*], Fajing Yang [a,c,*]

[a] Department of Vascular Surgery, The First Affiliated Hospital of Wenzhou Medical University, Wenzhou 325000, Zhejiang Province, PR China
[b] Department of Colorectal Surgery, The Second Affiliated Hospital of Zhejiang Chinese Medical University, Hangzhou 310000, PR China
[c] Key Laboratory of Diagnosis and Treatment of Severe Hepato-Pancreatic Diseases of Zhejiang Province, The First Affiliated Hospital of Wenzhou Medical University, Wenzhou 325000, PR China
[d] Department of Anesthesia, The First Affiliated Hospital of Wenzhou Medical University, Wenzhou 325000, Zhejiang Province, PR China
[e] Clinical Research Center, The First Affiliated Hospital of Wenzhou Medical University, Wenzhou 325000, PR China
[f] School of Pharmaceutical Sciences, Wenzhou Medical University, Wenzhou 325000, PR China

ARTICLE INFO

Keywords:
Egg white
Hydrogel
Chitosan
Sildenafil
Infected wound

ABSTRACT

Infected wounds are common clinical injuries that often complicated by inflammation and oxidative stress due to bacterial invasion. These wounds typically suffer from impaired vascularization, which delays healing and increases the risk of complications such as sepsis and chronic wounds. Therefore, developing an effective treatment for infected wounds is highly necessary. Egg white can promote cell regeneration and repair, while chitosan is effective in resisting bacterial invasion. Sildenafil is believed to have the potential to promote angiogenesis. Based on these properties, we have prepared a new type of hydrogel using egg white and chitosan as the framework, loaded with sildenafil (CEHS). The hydrogel combines the benefits of its components, exhibiting good biocompatibility and promoting the proliferation and migration of NIH 3T3 (3T3) cells and human umbilical vein endothelial cells (HUVEC), as well as the angiogenesis in HUVEC. It also exhibits significant antioxidant, anti-inflammatory, and antibacterial properties against *Escherichia coli (E. coli)* and *Staphylococcus aureus (S. aureus)*. Additionally, in a mouse model of infected wounds, the CEHS effectively promoted wound healing through its excellent antioxidant and anti-inflammatory properties, antibacterial activity, and pro-angiogenic effects. In summary, this simple-to-prepare, multifunctional natural hydrogel shows great promise for the treatment of infected wounds.

1. Introduction

Infected wounds are localized or systemic infections caused by the invasion of bacteria, fungi, or other microorganisms into open wounds (Abrahamian and Goldstein, 2011; Mo et al., 2022). They commonly occur in surgical incisions, diabetic foot ulcers, pressure sores, and burns (Webster et al., 2014). Among these, bacterial infections are the most prevalent, primarily caused by pathogenic bacteria such as *Escherichia coli (E. coli)* and *Staphylococcus aureus (S. aureus)* (Golan, 2019). These infections can delay healing, extend hospital stays, increase medical costs, and cause severe complications like sepsis and tissue death (Santoro et al., 2020; Su et al., 2017). The treatment of infected wounds is challenging and typically requires a comprehensive therapeutic strategy, including debridement, local management, application of antimicrobial dressings, and systemic or local antibiotic therapy (Li et al., 2022). Although these methods can control infections and promote healing to some extent, they still have numerous limitations. For example, the debridement process may cause additional tissue damage

* Corresponding authors at: Department of Vascular Surgery, The First Affiliated Hospital of Wenzhou Medical University, Zhejiang Province Wenzhou 325000, PR China.
** Corresponding author.
E-mail addresses: Wzzhangxiuhua@126.com (X. Zhang), 529365150@qq.com (D. Jia), 228927178@qq.com (W. Jin), yangfj25@126.com (F. Yang).
[1] These authors contributed equally to this work.

https://doi.org/10.1016/j.ijpx.2025.100328
Received 24 November 2024; Received in revised form 16 March 2025; Accepted 22 March 2025
Available online 24 March 2025

(Falabella, 2006), increasing patient pain and discomfort, and the issue of antibiotic resistance persists (Huemer et al., 2020). At present, commonly used wound dressings include films, foams, sponges, hydrogels, and nanofibers (Kumar et al., 2023a; Kumar et al., 2023b). Additionally, some novel materials, such as peptides delivered via nanocarriers, are also being investigated for wound treatment (Kumar et al., 2024).

In recent years, the application of hydrogels in the treatment of infected wounds has shown significant progress (Liang et al., 2021). Hydrogels offer several advantages, such as providing a moist healing environment, promoting tissue regeneration, and exhibiting good biocompatibility and drug delivery properties (Kesharwani et al., 2021). They can effectively release antimicrobial agents to inhibit microbial growth (Ng et al., 2014). Recent studies have demonstrated that functional hydrogels, such as silver-loaded hydrogels and bioactive molecule-loaded hydrogels, can significantly reduce the bacterial load in wounds and accelerate wound healing (Chu et al., 2023). Additionally, hydrogel patches have shown great potential in treating infected wounds (Jin et al., 2024a). However, the clinical application of hydrogels still faces several challenges, including cost, stability, and the feasibility of large-scale production (Chenani et al., 2024). Therefore, developing a novel hydrogel dressing that is cost-effective, efficient, and provides substantial therapeutic benefits for effectively treating infected wounds is of significant importance.

Natural polymer hydrogels are widely used in wound treatment due to their excellent biocompatibility, biodegradability, and moisturizing effects (Cai et al., 2024; Zhang et al., 2024a). Among these, egg white has received considerable attention owing to its low cost, easy availability, safety, and biological activity (Jalili-Firoozinezhad et al., 2020). Egg white is rich in proteins, which exhibit good biocompatibility and biodegradability, promoting cell adhesion and proliferation, thus facilitating wound healing (Dong and Zhang, 2021). Moreover, egg white is readily available, cost-effective, and easily prepared for large-scale production (Xiao et al., 2021). Egg white hydrogels also exhibit favorable mechanical properties and moisturizing effects, providing a moist healing environment for wounds and reducing scar formation (Rafati et al., 2020). Chitosan, a natural polysaccharide, has shown significant advantages in the treatment of infected wounds due to its excellent antibacterial properties (Abd El-Hack et al., 2020). The cationic nature of chitosan allows it to interact with bacterial cell membranes, leading to membrane disruption and inhibition of bacterial growth (Helander et al., 2001). Chitosan hydrogels can effectively suppress bacterial growth, reduce the risk of wound infection, and promote wound healing and tissue regeneration (Liu et al., 2018). In summary, combining egg white and chitosan as raw materials for hydrogel preparation can enhance the mechanical properties of the hydrogel. The adjustable viscosity and biological activity of these materials provide a suitable moist microenvironment for wounds, offering multiple functional advantages. Furthermore, the high economic efficiency and safety of egg white and chitosan make them ideal choices for the treatment of infected wounds.

Sildenafil, a phosphodiesterase-5 inhibitor, has garnered significant attention in recent years for its applications in wound healing and the treatment of infected wounds (ElHady et al., 2023). Its mechanism of action is likely through the increase of nitric oxide and cyclic guanosine monophosphate levels, which promote the relaxation of vascular endothelial cells and the formation of new blood vessels (Halcox et al., 2002; Yang et al., 2024). This, in turn, improves blood circulation and oxygen supply in the wound area, accelerating tissue repair and the wound healing process. Additionally, sildenafil has significant anti-inflammatory and antioxidant effects that reduce the inflammatory response in wounds, promoting cell proliferation and collagen synthesis (Ding et al., 2024; Ma et al., 2024). These biological effects not only help to accelerate the healing of non-infected wounds but also show important potential in the treatment of infected wounds. Therefore, the potential application value of sildenafil in the treatment of infected wounds is highly regarded and warrants further research and development. Combining these findings with the advantages of natural polymer hydrogels, such as egg white and chitosan, may lead to the development of advanced hydrogel dressings with multiple therapeutic functions, including improved blood flow, anti-inflammatory, and antibacterial properties, thereby enhancing the overall effectiveness and safety of treatments for infected wounds.

Hence, we designed a novel hydrogel for the treatment of infected wounds. The hydrogel, primarily composed of egg white and chitosan, is loaded with sildenafil and prepared using a simple and cost-effective method, resulting in a chitosan-egg white hydrogel loaded with sildenafil (CEHS). In the treatment of infected wounds, CEHS retains the inherent functionalities of its two main components while also leveraging the significant effects of sildenafil. CEHS exhibits excellent mechanical strength and degradation properties. In vitro cell experiments have demonstrated its good biocompatibility, promoting the proliferation and migration of fibroblasts and endothelial cells, as well as endothelial cell tubulogenesis, while inhibiting oxidative stress and inflammatory responses in macrophages. CEHS also shows effective antibacterial activity against *E. coli* and *S. aureus*. To further validate the anti-inflammatory, antioxidant, antibacterial, and pro-angiogenic effects of CEHS, we conducted in vivo experiments using a murine model of infected wounds. These experiments confirm that CEHS promotes the healing of burn wounds by reducing inflammation, oxidative stress, and bacterial load, and by enhancing angiogenesis. In summary, CEHS has demonstrated significant potential in the treatment of infected wounds, offering new insights and methods for clinical applications in this field.

2. Materials and methods

2.1. Materials

Fresh eggs were sourced from a local supermarket. Chitosan (Powder, molecular weight: 50,000–190,000 Da, viscosity: 20–300 cP) and Dulbecco's Modified Eagle Medium (DMEM) were obtained from Sigma, Sildenafil and NaOH was purchased from Aladdin. Cell Counting Kit-8 (CCK-8), Calcein/PI Cell Viability/Cytotoxicity Assay Kit, Reactive Oxygen Species Assay Kit for Superoxide Anion with Dihydroethidium (DHE) and Reactive Oxygen Species Assay kit were both purchased from Beyotime. Lipopolysaccharide (LPS) and phosphate buffered solution (PBS) was obtained from Solarbio. Nutritious broth was purchased from Huan Kai Microbial. Mouse TNF-α Enzyme-Linked Immunosorbent Assay (ELISA) Kit, Mouse IL-1β ELISA Kit, and Mouse TGF-β1 ELISA Kit were all purchased from Multi Sciences (Lianke) Biotech Co., Ltd. The Superoxide Dismutase (SOD) assay kit, Malondialdehyde (MDA) assay kit, and Hydroxyproline (HYP) assay kit were all procured from Nanjing Jiancheng Bioengineering Institute. The α-smooth muscle actin (α-SMA) antibody, platelet endothelial cell adhesion molecule-1 (CD31) antibody, and vascular endothelial growth factor (VEGF) antibody were all obtained from Abcam.

HUVEC,NIH 3T3 and RAW 264.7 obtained from the Wuhan Procell Biotechnology Co., Ltd. *E. coli* and *S. aureus* were acquired from Shanghai North Connaught biotechnology Co., Ltd.

2.2. Methods

2.2.1. Synthesis of chitosan-egg white hydrogel loaded with sildenafil (CEHS)

Synthesise CEHS by referencing the synthetic methods from previous literature and making appropriate improvements (Chang et al., 2019). Carefully separate the egg white from fresh eggs and thoroughly stir it to obtain a uniform liquid consistency. Add the egg white solution to a solution containing 2 wt% (*w/v*) sildenafil, 3 wt% (w/v) chitosan, and 0.5 M NaOH, ensuring the two solutions are mixed in a 1:1 volume ratio. Allow the mixture to gel, and then immerse it in Dulbecco's Modified Eagle Medium (DMEM) for 12 h to promote secondary cross-linking. The resultant product is a chitosan-egg white hydrogel loaded with sildenafil

(CEHS). For comparison, a chitosan-egg white hydrogel (CEH) without sildenafil was prepared using an analogous method.

2.2.2. Characterization of CEHS

To characterize the CEHS, its morphology and microstructure were observed using a scanning electron microscope (SEM, Hitachi Regulus8100). The hydrogel samples were lyophilized, then sputter-coated with a thin layer of gold, and observed using SEM operated at 5.00 kV. The lyophilized samples of CEH and CEHS were analyzed by fourier transform infrared spectroscopy (FTIR, Nicolet iS 10) in the range of 4000 to 400 cm^{-1}.

2.2.3. Degradation experiments

The hydrogel samples were cut into appropriate dimensions (length: 1 cm, width: 1 cm, height: 0.3 cm) and their initial weights (W_0) were measured using a precision balance. Subsequently, the hydrogel samples were immersed in PBS solution and maintained at room temperature. At predetermined intervals (respectively, 2 h, 4 h, 6 h, 12 h, 24 h, 48 h, 72 h), the hydrogel samples were retrieved, gently blotted dry with filter paper to remove surface moisture, and then weighed (W_1) (Zhang et al., 2024b). Each group was repeated triplicate. The degradation ratio was calculated using the formula: Degradation ratio = (W_0 - W_1) / W_0 * 100 %.

2.2.4. Swelling experiments

The hydrogel samples were cut into appropriate dimensions (length: 1 cm, width: 1 cm, height: 0.3 cm), lyophilized and weighed (M_0). Then, the samples were immersed in PBS at room temperature. At predetermined time intervals (respectively, 2 h, 4 h, 6 h, 12 h, 24 h, 48 h, 72 h), the samples were removed and reweighed (M_1) (Gao et al., 2023). Each group was repeated triplicate. The swelling ratio was calculated using the formula: Swelling ratio = (M_1 - M_0) / M_0 * 100 %.

2.2.5. Rheological characterization of CEHS

The rheological properties of the hydrogels were measured at room temperature using a rheometer (DHR-2, TA) equipped with a 10 mm diameter parallel plate rotor. Oscillatory strain sweep from 0.1 % to 100 % at an angular frequency of 10 rad·s^{-1} was performed. The viscosity of the hydrogel was determined by scanning the shear rate from 0.1 to 20 s^{-1}(Jin et al., 2024a). Each group was tested triplicate.

2.2.6. In vitro drug release study

To evaluate the in vitro drug release capabilities of CEHS hydrogel, the 100 mg samples were placed in dialysis bags with a molecular weight cutoff of 12,000–14,000 Da and immersed in PBS at 37 °C. The dialysis bags were then placed on a shaker and gently agitated. At predetermined time points (respectively, 1 h, 2 h, 4 h, 8 h, 12 h, 24 h, 48 h, 72 h), 200 μL of the supernatant was sampled and immediately replaced with an equal volume of fresh PBS. The collected supernatant was analyzed for the concentration of sildenafil released using a UV spectrophotometer (Cary 3500, Agilent Technologies) at a wavelength of 280 nm. Each group was repeated triplicate.

2.2.7. Cytocompatibility assay

To evaluate the cytotoxicity of CEHS hydrogel on cells, we selected fibroblasts (3T3) and endothelial cells (HUVEC), which are the most common and predominant cell types in wounds, as the subjects of our study (Shrestha et al., 2024). After the hydrogel fully formed, it was soaked in PBS for 8 h to collect the corresponding hydrogel elution. The extraction method was subsequently applied to prepare hydrogel leachates for all subsequent experiments. The cytotoxic effects of the CEHS hydrogel on 3T3 cells and HUVEC were assessed using the Cell Counting Kit-8 (CCK-8, Beyotime). First, the cells were seeded in 96-well plates. Afterward, 20 μL of hydrogel eluate or an equal volume of PBS was added to each well. The plates were incubated for 24, 48, and 72 h. Then, the old culture medium was discarded, and the cells were washed three times with PBS. Subsequently, 20 μL of CCK-8 solution was added to each well and incubated for 1 h. Following incubation, the absorbance at 450 nm was measured for each well using a microplate reader (Varioskan LUX, Thermo Fisher Scientific). Each group was tested triplicate. Finally, at 72 h, Calcein/PI staining was performed to fluorescently label the cells. The cells were incubated with 100 μL of Calcein-AM and 100 μL of PI for 30 min at 37 °C. After staining, the cells were washed three times with PBS to remove excess dye. The staining conditions were assessed using fluorescence microscopy (TE2000-U, Nikon) at excitation/emission wavelengths of 490/520 nm for Calcein-AM and 535/617 nm for PI. Representative images (n = 3 per group) were captured to evaluate the viability and morphology of the cells.

2.2.8. Scratching experiment

HUVEC or 3T3 cells were cultured in 6-well plates until reaching 100 % confluence, and scratches were made using a 200 μL pipette tip. The cells were then cultured in serum-free DMEM containing 200 μL of hydrogel eluate or an equal volume of PBS. Cell migration was observed and recorded at 0, 12, and 24 h. Wound closure was assessed by comparing the scratch areas at 0, 12, and 24 h. Each group was repeated triplicate. The quantification of wound closure was calculated using the following formula: Wound Healing Rate = (0 h Scratch Area − 12 h or 24 h Scratch Area) / 0 h Scratch Area * 100 %.

2.2.9. Tube formation experiment

Fifty microliters of Matrigel (ABW 0827245) were plated in each well of a 24-well plate and incubated at 37 °C for 30 min. HUVEC were seeded at a density of 1 × 10^5 cells per well and treated with culture medium containing 200 μL of hydrogel eluate or an equal volume of PBS. HUVEC were stained with Calcein-AM. Tubule formation by HUVEC was observed at 8 h using a microscope (TE2000-U, Nikon), and the number of tubules formed in each group was quantified. Each group was repeated triplicate.

2.2.10. Antioxidant activity

RAW 264.7 cells were cultured in 6-well plates until they reached 90 % confluence. Subsequently, 1 mL of 50 mg/mL Rosup was added to each well to simulate an oxidative stress environment, followed by the addition of 200 μL of hydrogel extract or an equivalent volume of PBS for co-culturing with the cells for 6 h. Afterward, the old culture medium was aspirated, and the cells were washed three times with PBS. Each well was then stained with 1 mL of 10 μM DCFH-DA probe for 30 min to detect intracellular reactive oxygen species (ROS) levels. Finally, the cells were collected, and the fluorescence intensity was measured using flow cytometry. Each group was repeated triplicate.

2.2.11. Anti-inflammatory activity

RAW 264.7 cells were cultured in 24-well plates until they reached 90 % confluence. Subsequently, 0.5 mL of 1 μg/mL LPS was added to each well to induce an inflammatory environment (Jin et al., 2024b). The cells were then treated with 200 μL of hydrogel extract or an equivalent volume of PBS for co-culturing for 24 h. After the incubation period, 200 μL of the cell supernatants were collected and the levels of TNF-α and IL-1β were measured using commercial ELISA kits. Each group was repeated sextuplicate.

2.2.12. Antibacterial capacity

The antibacterial activity of the CEHS hydrogel against *E. coli* and *S. aureus* were evaluated. *E. coli* and *S. aureus* were cultured in broth medium and incubated at 37 °C in an incubator. Fifty milligrams of CEHS hydrogel was added to a suspension of *Staphylococcus aureus* (1.0 × 10^5 CFU/mL) and incubated for 24 h. For the control group, PBS was added. Finally, 20 μL of the bacterial suspension was plated on agar plates and incubated at 37 °C for 24 h. The plates were then removed, and the observations were recorded and photographed. In addition, 100 μL of bacterial suspension was taken and its OD value was measured at a

wavelength of 600 nm using a microplate reader. Each group was repeated triplicate. The inhibition rate was calculated using the following formula:

Inhibition rate = (Control Group OD value - Experimental Group OD value) / Control Group OD value * 100 %.

2.2.13. Infected wound animal model

In this study, wild-type C57BL/6 male mice (6–8 weeks old) weighing 20–25 g were obtained from Zhejiang Vital River Laboratory Animal Technology Co., Ltd. All mice were housed in cages within the clean-grade animal facility of the First Affiliated Hospital of Wenzhou Medical University. The environmental conditions in the facility were maintained at an indoor temperature of approximately 21 °C with a daily temperature variation of ±3 °C and a humidity level of 50 % at the cage level. The mice were kept on a 12 h light/12 h dark cycle and had ad libitum access to food and water. All experimental procedures were conducted in accordance with the animal ethical guidelines approved by the Ethics Committee of the First Affiliated Hospital of Wenzhou Medical University and the Experimental Animal Management Committee of Zhejiang Province (Approval No.: WYYY-IACUC-AEC-2024-091).

The animal studies was conducted using a full-thickness infected wound model in mice (Cheng et al., 2023; Qiao et al., 2023). Twenty-four mice were randomly divided into three groups: (1) control group, (2) CEH experimental group, and (3) CEHS experimental group, with 8 mice in each group. All mice were anesthetized with 3 % sodium pentobarbital (50 mg/kg) and had their backs depilated. A 10 mm diameter skin biopsy punch was used to create a 10 mm circular full-thickness skin wound on the back of each mouse. A *S. aureus* suspension (200 μL, 1×10^8 CFU/mL) was then applied to the wound. The model was considered successfully established if the wound showed visible signs of infection and the presence of *S. aureus* was confirmed (Heunis et al., 2013). A 10 mm diameter circular hydrogel patch was applied to the infected wound on the back of each mouse. Wound images were taken on days 1, 3, 5, 10, and 15 using a camera, and the wound area was measured using ImageJ software. Each group was tested in triplicate. The wound healing rate was calculated using the following formula: Wound healing rate = $(A_0 - A_1) / A_0 * 100$ %, where A_0 is the initial wound area and A_1 is the actual wound area at a specified time.

2.2.14. Histological staining

Skin wound tissue samples from the dorsal side of mice were collected on days 5 and 15 from each group. The samples were fixed in 4 % paraformaldehyde, embedded in paraffin, and sectioned at a thickness of 4 μm according to standard histological procedures. The sections were routinely stained with hematoxylin and eosin (HE) for histological examination and with Masson's trichrome to assess collagen deposition in the wound. Immunohistochemical (IHC) staining was performed for α-SMA (1:200), CD31 (1:200), and VEGF (1:200) in the wound tissues following standard protocols. The sections were finally observed under an optical microscope, and quantitative analysis was performed using ImageJ software. Each group was tested in triplicate.

2.2.15. ROS assessment

To evaluate the ROS levels in wound tissue, the samples from wounded mice were rapidly frozen in liquid nitrogen and embedded in optimal cutting temperature (OCT) compound. The embedded tissue blocks were sectioned at a thickness of 8 μm using a cryostat. The sections were then fixed with 4 % paraformaldehyde for 1 h at room temperature. Following fixation, the sections were stained with 10 μM dihydroethidium (DHE) for 30 min and counterstained with 4′,6-diamidino-2-phenylindole (DAPI) for 3 min. The slides were observed and photographed using a fluorescence microscope, and quantitative analysis was performed using ImageJ software. Each group was tested in triplicate.

2.2.16. Enzyme-linked immunosorbent assay (ELISA)

Skin wound tissue samples were collected from the dorsal region of mice on days 5 and 15 for each group. The skin tissue was washed with pre-chilled PBS, and 20 mg of the tissue was cut into small pieces. According to a weight to volume ratio of 1:9, each 1 mg of tissue sample corresponds to 9 μL of PBS. One millimolar PMSF (phenylmethylsulfonyl fluoride) was added, and the mixture was thoroughly ground on ice. Subject the homogenate to ultrasonic disruption. Finally, centrifuge the homogenate at 8000 rpm for 5 min at 4 °C, and collect the supernatant for analysis. Subsequently, corresponding ELISA kits were used to quantitatively measure the levels of TNF-α, IL-1β, and TGF-β in the supernatant. All procedures were conducted according to the manufacturer's instructions. Four replicates were performed for each group.

2.2.17. Concentrations of SOD, MDA, and HYP in the wound tissue

Skin wound tissue samples were collected from the dorsal region of mice on days 5 and 15 for each group. Twenty milligrams of skin tissue were accurately weighed. Nine times the volume of PBS was added at a weight (g) to volume (mL) ratio of 1:9. Mince the tissue and prepare a homogenate in an ice bath. Centrifuge at 4000 rpm for 10 min, and collect the supernatant, which represents the 10 % homogenate supernatant for subsequent analysis. According to the manufacturer instructions, appropriate assay kits were used to evaluate the activity of superoxide dismutase (SOD), the levels of malondialdehyde (MDA), and the content of hydroxyproline (HYP). Each group was tested in triplicate.

2.2.18. In vivo antibacterial activity

To collect wound tissue samples from the dorsal skin of mice at 5 and 15 days post-injury, the wound tissue was excised using sterile scissors and forceps, placed in sterile containers, and weighed to obtain 10 mg. The tissue samples were then cut into small pieces and ground to ensure the complete release of bacteria. The ground tissue was transferred to sterile tubes and mixed with an appropriate volume of sterile PBS. The tissue homogenate was diluted 50-fold and centrifuged at 3000 rpm for 10 min. The supernatant was discarded, and the pellet was resuspended in sterile PBS to create a bacterial suspension. One hundred microliters of the bacterial suspension was added to each well of a 96-well plate, and the OD was measured at 600 nm using a microplate reader. Each group was tested in quadruplicate. All procedures were performed under sterile conditions to prevent contamination.

2.2.19. Statistical analysis

The experimental data are presented as mean ± standard deviation (SD). One-way analysis of variance (ANOVA) was used to assess differences between groups. Statistical significance is indicated as follows: $^*p < 0.05$, $^{**}p < 0.01$, $^{***}p < 0.001$, $^{****}p < 0.0001$; "ns" denotes no significant difference. All experiments were performed at least three times ($n = 3$).

3. Results and discussion

3.1. Preparation and Characterization of CEHS

The chitosan-egg white hydrogel loaded with sildenafil (CEHS) was prepared using a simple and cost-effective method (Chang et al., 2019; Wang et al., 2022) (Fig. 1). The final product is the CEHS (Fig. 2A). First, the microstructure of CEHS was observed using scanning electron microscopy (SEM), revealing a relatively uniform porous network structure (Fig. 2B). Subsequently, both CEH and CEHS were lyophilized, and their Fourier transform infrared (FTIR) spectra were analyzed. The results indicated that CEHS exhibited characteristic peaks around 900 cm^{-1} and broad peaks in the range of 3100–3400 cm^{-1}, which are attributed to the carbohydrate structures in the hydrogel. Additionally, the absorption peak at 1460 cm^{-1} is associated with the bending and asymmetric deformation of the CH_3 groups in the hydrogel (Chang et al., 2019;

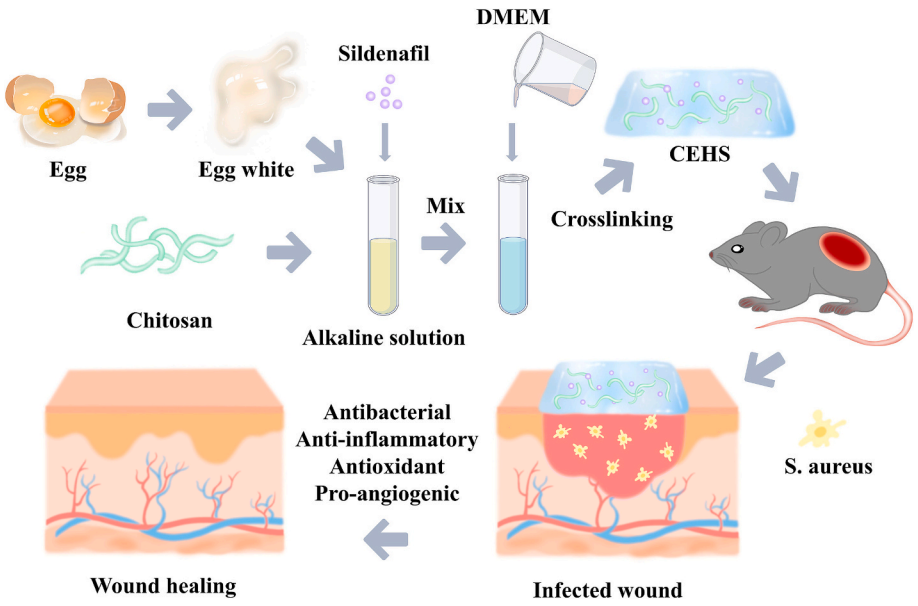

Fig. 1. Schematic diagram of the preparation of chitosan-egg white hydrogel loaded with sildenafil (CEHS) and its application in treating infected wounds in mice.

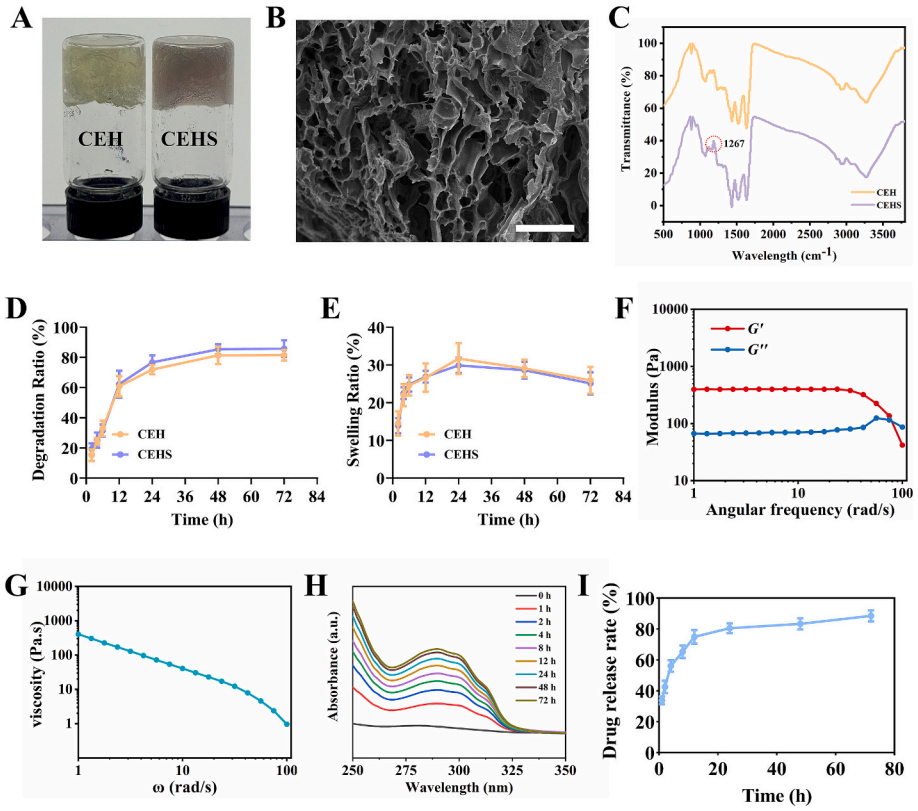

Fig. 2. Characterization of CEHS. (A). Physical photographs of CEH and CEHS. (B). Transmission electron microscopy (TEM) picture of CEHS. Scale bar is 50 μm. (C). FITR of CEH and CEHS. (D). Degradation ratio of CEH and CEHS in PBS ($n = 3$). (E). Swelling ratio of CEH and CEHS in PBS (n = 3). (F). Storage (G') and loss (G") modulus of the CEHS. (G). Shear viscosity of CEHS. (H). UV-spectroscopy investigation of the absorbance of sildenafil released from CEHS at a wavelength of 290 nm over different time intervals in vitro. (I). In vitro release of sildenafil from CEHS in PBS ($n = 3$).

Justin and Chen, 2014). The addition of sildenafil introduced a new peak near 1267 cm^{-1} in the FTIR spectra of the hydrogel samples (Li et al., 2009), confirming the successful incorporation of sildenafil into the hydrogel (Fig. 2C). The degradation ability of the hydrogels was assessed through a degradation test, and CEHS showed a degradation rate of nearly 80 % after immersion in PBS for 24 h. This result indicates that CEHS have excellent degradation properties under biologically relevant conditions (Fig. 2D). The CEHS possesses a porous network structure, which provides the foundation for absorbing exudate and maintaining a moist healing environment. The swelling behavior of lyophilized CEHS was evaluated through a swelling test, and the results showed that the swelling ratio reached a peak of 29.86 ± 2.01 % after

24 h of immersion in PBS (Fig. 2E). After 24 h, the swelling ratio gradually decreased at a slower rate, indicating that CEHS has a high initial swelling capacity and relatively stable swelling properties in PBS. This absorption capability allows CEHS to provide a stable moist environment for wound healing.

The frequency-dependent storage modulus (G') and loss modulus (G") were analyzed to confirm the typical viscoelastic properties of CEHS (Fig. 2F). Beyond a certain range, CEHS rapidly collapses, which is crucial for wound dressing applications as it helps the hydrogel provide appropriate support and recoverability upon contact with the wound. With increasing shear rate, the viscosity of CEHS decreases, exhibiting typical shear-thinning rheological behavior (Fig. 2G). This property ensures that the hydrogel can be more uniformly distributed across the wound tissue during practical applications (Unterman et al., 2017). The release profile of sildenafil from CEHS was determined by immersing CEHS in PBS and measuring the sildenafil concentration in the supernatant at various time points using UV spectroscopy (Fig. 2H). The results indicated that sildenafil was released rapidly within the first 12 h, followed by a gradual decrease in the release rate until a steady state was reached (Fig. 2I). This release characteristic is beneficial for quickly achieving a high therapeutic dose of sildenafil in a short period, followed by sustained release, which can prolong the drug action time. This helps reduce the frequency of drug administration and maintain therapeutic efficacy.

In summary, the excellent degradation properties of CEHS allow it to gradually degrade during the wound healing process, reducing the pain

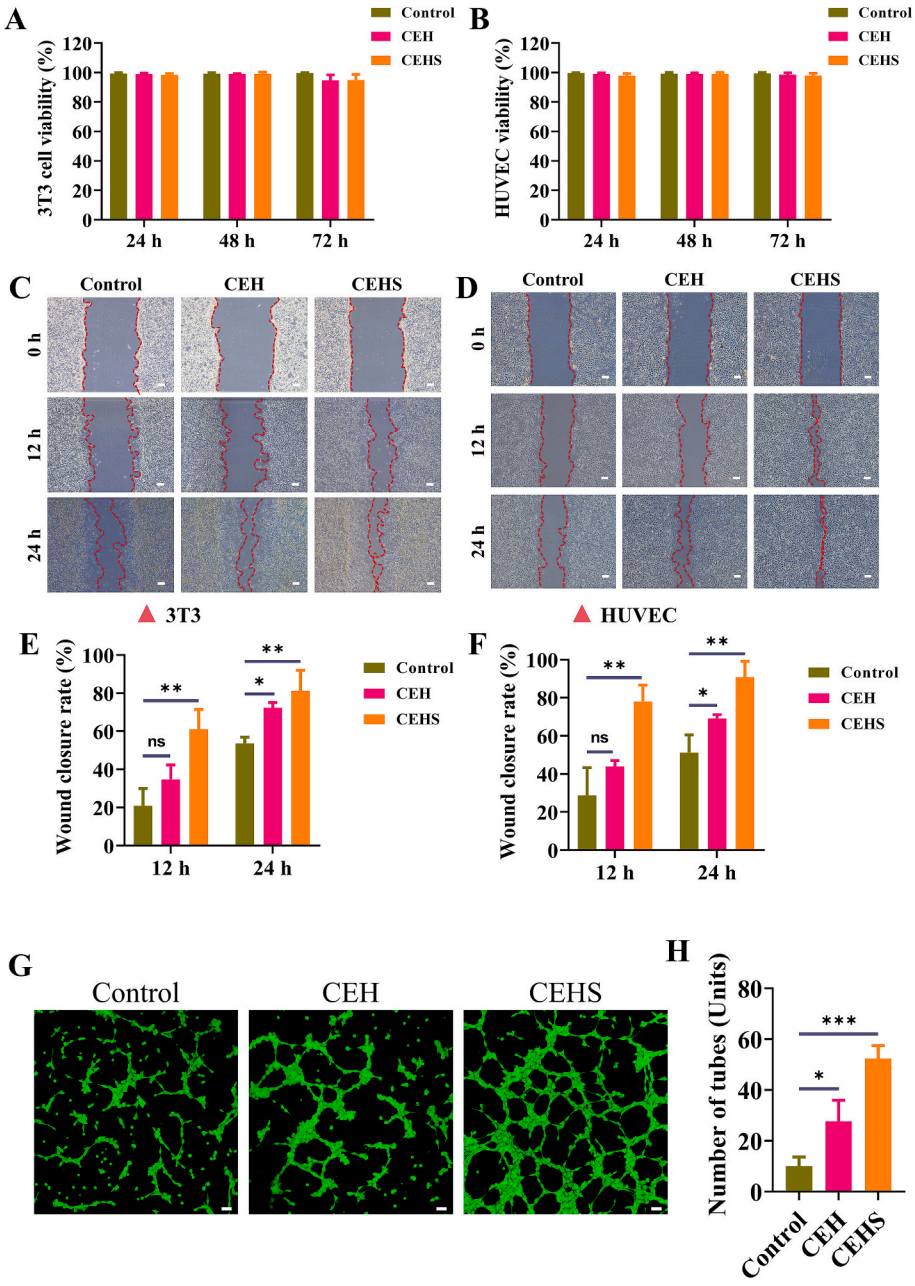

Fig. 3. Cell compatibility and cell assays of CEHS. (A). CCK-8 assay of cell viability after co-incubation of CEHS with 3T3 ($n = 4$). (B). CCK-8 assay of cell viability after co-incubation of CEHS with HUVEC (n = 4). (C). Images of in vitro scratch assays of 3T3 after different treatments. Scale bar is 100 μm. (D). Images of in vitro scratch assays of HUVEC after different treatments. Scale bar is 100 μm. Wound closure rates of 3T3 (E) and HUVEC (F) after different treatments in a wound healing model (n = 3). (G). Tube formation assay of HUVEC after different treatments in vitro. Scale bar is 50 μm. (H). Quantitative analysis of tube formation in the tube formation assay (n = 3). All data are shown as the mean ± SD. Compared with control group, ns ≥ 0.05, *$p < 0.05$, **$p < 0.01$, ***$p < 0.001$.

and risk associated with the removal of dressings. Additionally, the moderate swelling properties enable the hydrogel to better conform to the wound, forming an effective barrier that prevents external bacterial infection and wound dehydration. Furthermore, the mechanical strength of CEHS is sufficient to support the protection and repair of the wound. The drug release characteristics of CEHS not only optimize the drug utilization efficiency but also reduce the frequency of drug administration, enhancing the overall safety and efficacy of the treatment. Collectively, these properties make CEHS an ideal wound healing material with broad application prospects and clinical value.

3.2. The cellular compatibility and interaction of CEHS in vitro

Cell compatibility is a prerequisite for material application (Jin et al., 2024b). Fibroblasts and endothelial cells are important components of skin tissue; therefore, they are commonly used to evaluate the biocompatibility of hydrogels for wound applications (Barros et al., 2021; Naahidi et al., 2017). In this study, we selected 3T3 and HUVEC cells as the subjects of our investigation. The cytotoxicity of CEHS was evaluated using the CCK-8 assay (Fig. 3A, B). Specifically, the extract of CEHS was co-cultured with the cells, and cell viability was measured continuously over three days. There was no significant difference in cell viability between the CHE and CEHS experimental groups and the control group. Additionally, on the third day, live-dead staining was performed for cells in each group (Figs. S1A, S1B) to visually demonstrate the cell viability status. The staining results showed that the majority of cells in both the CHE and CEHS experimental groups maintained good viability. These experimental results indicate that CEHS has excellent cytocompatibility and low toxicity, making it suitable for use as a biomaterial in tissue engineering applications.

The scratch assay is commonly used to simulate the wound healing process and evaluate cell migration and wound closure capabilities (Bobadilla et al., 2019), which is of great significance for studying the promotion of wound healing by CEHS at the cellular level. The results of the scratch assay demonstrate that the addition of CEHS significantly enhances cell migration speed and wound coverage ability (Fig. 3C, D). Specifically, compared to the control group, the wound closure rates in the CHE and CEHS experimental groups were higher, with the 3T3 cells and HUVEC achieving wound closure rates of over 80 % and 90 %, respectively, within 24 h (Fig. 3E, F). The distribution of cells in the wound area was more uniform and dense. These findings indicate that CEHS effectively promotes cell migration and proliferation, playing a crucial positive role in the wound healing process. Endothelial cell tube formation is a critical step in angiogenesis during the wound healing process, promoting blood supply and tissue repair, and accelerating wound healing (Tonnesen et al., 2000). The results of the tube formation assay show that, compared to the control group without hydrogel, HUVEC in the CEH and CEHS experimental groups formed more and longer tubular structures after the addition of hydrogel. These tubular structures not only increased in number but also exhibited more regular and stable morphology (Fig. 3G). The number of tubular structures in the CEHS experimental group reached 52.33 ± 5.13 (Fig. 3H). These results indicate that CEHS significantly enhances the tube formation ability of endothelial cells, promoting the formation of new blood vessels and thereby accelerating the wound healing process.

Additionally, through 5-Ethynyl-2′-deoxyuridine (EdU) staining of 3T3 cells and HUVEC, we observed a marked increase in fluorescence intensity in the CEHS group compared to the control group (Figs. S2A, S2C). Quantitative analysis of the fluorescence images showed that the EdU fluorescence intensity in the CEHS group was enhanced by 39.32 ± 3.03 % and 46.22 ± 5.04 % for 3T3 cells and HUVEC, respectively, compared to the control group (Figs. S2B, S2D). These results clearly demonstrate that CEHS has a strong ability to promote cell proliferation.

In summary, CEHS not only exhibits good cell compatibility and low toxicity but also significantly enhances cell migration, proliferation, and endothelial cell tube formation, thereby accelerating the wound healing process.

3.3. In vitro performance of CEHS

In the treatment of infected wounds, ROS, inflammation, and bacteria pose the three major challenges we must address. These factors interact with and exacerbate one another, profoundly influencing the wound healing process and treatment outcomes (Mamun et al., 2024; Wilkinson and Hardman, 2020). Therefore, utilizing wound dressings with antioxidant, anti-inflammatory, and antibacterial properties can effectively address these multiple challenges, significantly enhancing the treatment efficacy of infected wounds. RAW 264.7 cells serve as a classic macrophage model and are widely used in studies of oxidative stress and inflammation (Castaneda et al., 2017). To simulate an oxidative stress environment, RAW264.7 cells were treated with Rosup, followed by the addition of hydrogel eluates. The cells were then stained with DCFH-DA probe to detect intracellular ROS levels. Fluorescence intensity was measured using flow cytometry, and the results showed a significant reduction in fluorescence intensity in the CEH and CEHS experimental groups compared to the control group (Fig. 4A). Specifically, the fluorescence intensity in the CEHS group was reduced by 50.06 ± 14.77 compared to the control group (Fig. 4B), indicating that CEHS can effectively decrease ROS levels in RAW264.7 cells under oxidative stress conditions, demonstrating its potent antioxidant capacity. To simulate an inflammatory environment, RAW264.7 cells were stimulated with lipopolysaccharide (LPS), inducing the secretion of various inflammatory mediators (such as TNF-α and IL-1β) to mimic an in vivo inflammatory state (Chen et al., 2021). The cells were subsequently exposed to hydrogel eluates or PBS solution to evaluate the regulatory effects of CEHS on cellular inflammatory responses. ELISA was used to measure the concentrations of TNF-α and IL-1β in the supernatants of each group. The results indicated that both the CEH and CEHS experimental groups had significantly reduced concentrations of TNF-α and IL-1β compared to the control group. Specifically, the CEH group had TNF-α and IL-1β concentrations reduced to 223.87 ± 17.17 and 131.26 ± 20.74 pg/mL, respectively, while the CEHS group had concentrations reduced to 217.33 ± 22.75 and 138.57 ± 16.83 pg/mL, respectively (Fig. 4C, D). These findings suggest that CEHS can effectively suppress inflammatory responses in RAW264.7 cells under inflammatory conditions, demonstrating its strong anti-inflammatory properties. Furthermore, to further validate the protective effect of CEHS on cells, we simultaneously added the oxidative stress inducer Rosup and the inflammation inducer LPS to the cell cultures, thereby establishing a dual-stimulation model of oxidative stress and inflammation. Subsequently, the cells were co-cultured with CEHS, and the protective effect of CEHS was assessed by measuring cell viability. The experimental results indicated that the cell protective rate in the CEHS group was the highest among the 3T3, HUVEC, and RAW 264.7 cell lines (Figs. S3A, S3B, S3C), suggesting that CEHS exerts a significant protective effect on cells.

E. coli and *S. aureus* are the most common bacteria in the skin microenvironment. Therefore, we chose these two bacterial species to evaluate the antibacterial activity of CEHS in vitro. Agar plate assay results showed a clear antibacterial effect against both *E. coli* and *S. aureus* (Fig. 4E). The antibacterial activities of CEHS against *E. coli* and *S. aureus* were respectively 70.37 ± 3.42 % and 84.82 ± 2.48 % (Fig. 4F, G). This indicates that CEHS possesses significant broad-spectrum antibacterial properties and can effectively inhibit these common pathogens.

As an innovative hydrogel material, CEHS demonstrated exceptional biological activity in addressing the multifaceted challenges of oxidative stress, inflammation, and bacterial infection, showcasing excellent antioxidant, anti-inflammatory, and antibacterial capabilities.

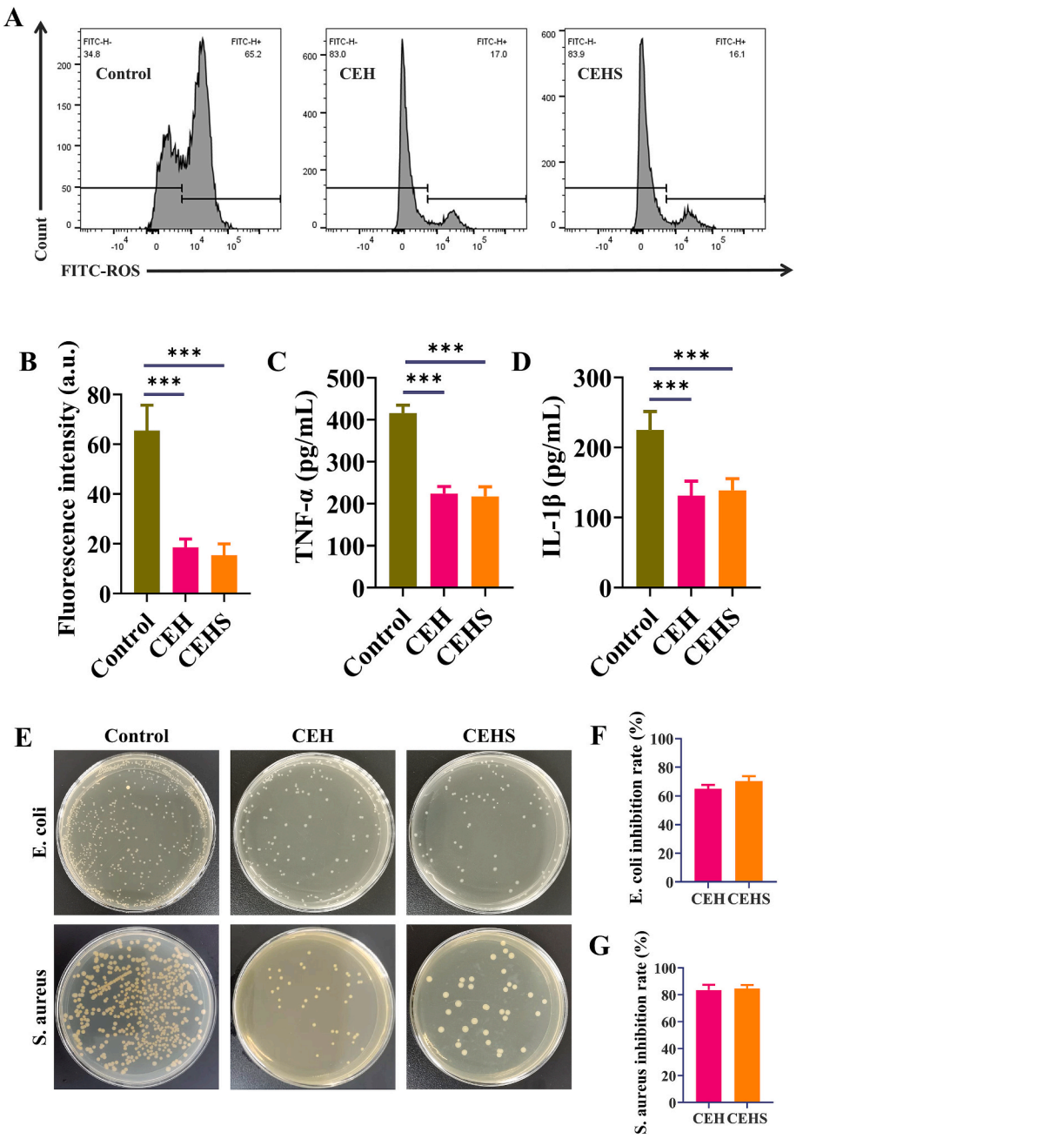

Fig. 4. In vitro performance of CEHS. (A). Flow cytometry analysis of ROS intensity in RAW264.7 cells after different treatments. (B). Quantitative analysis of ROS intensity corresponding to Fig. (A) (n = 3). Effects of different treatments on the levels of inflammation factors TNF-α (C) and IL-1β (D) in LPS-induced RAW264.7 cells ($n = 6$). (E). Survival images of *E. coli* and *S. aureus* on agar plates after different treatments. Bacterial inhibition rates of *E. coli* (F) and *S. aureus* (G) after different treatments (n = 4). All data are shown as the mean ± SD. Compared with control group, ns ≥ 0.05, *p < 0.05, **p < 0.01, ***p < 0.001.

3.4. Healing efficacy of CEHS in infected wounds in mice

In vitro experiments preliminarily validated the potential of CEHS in treating infected wounds. Therefore, this study employed a mouse model of full-thickness skin infection to further verify the efficacy of CEHS. Male mice were divided into three groups: a control group (no intervention), a CEH group (treated with CEH), and a CEHS group (treated with CEHS). The overall experimental procedure is shown in Fig. 5A. Wound healing was monitored by photographing the wounds at days 3, 5, 7, and 10, after the wounds were either left untreated or covered with the corresponding hydrogel. On day 5, the wound healing rates for the CEH and CEHS groups were 49.61 ± 4.43 % and 62.68 ± 7.01 %, respectively. By day 15, the CEHS group exhibited nearly complete wound healing, with significantly better wound closure compared to the CEH group and the control group (Fig. 5B, C). This indicates that CEHS has a significant advantage in promoting the healing of infected wounds. Analyzing the changes in wound healing rates, the CEHS group was the first to approach 100 % healing (Figure S4A), indicating that CEHS is the most effective in promoting the healing of infected wounds. To further validate the therapeutic effects of CEHS, histopathological analysis was performed using HE and Masson staining on the wound tissues from each group (Fig. 5D). HE staining results showed that in the early stages of wound healing (day 5), the control group exhibited significant inflammatory cell infiltration, whereas both the CEH and CEHS groups showed a marked reduction in the number of inflammatory cells. This reduction suggests that CEHS plays a crucial

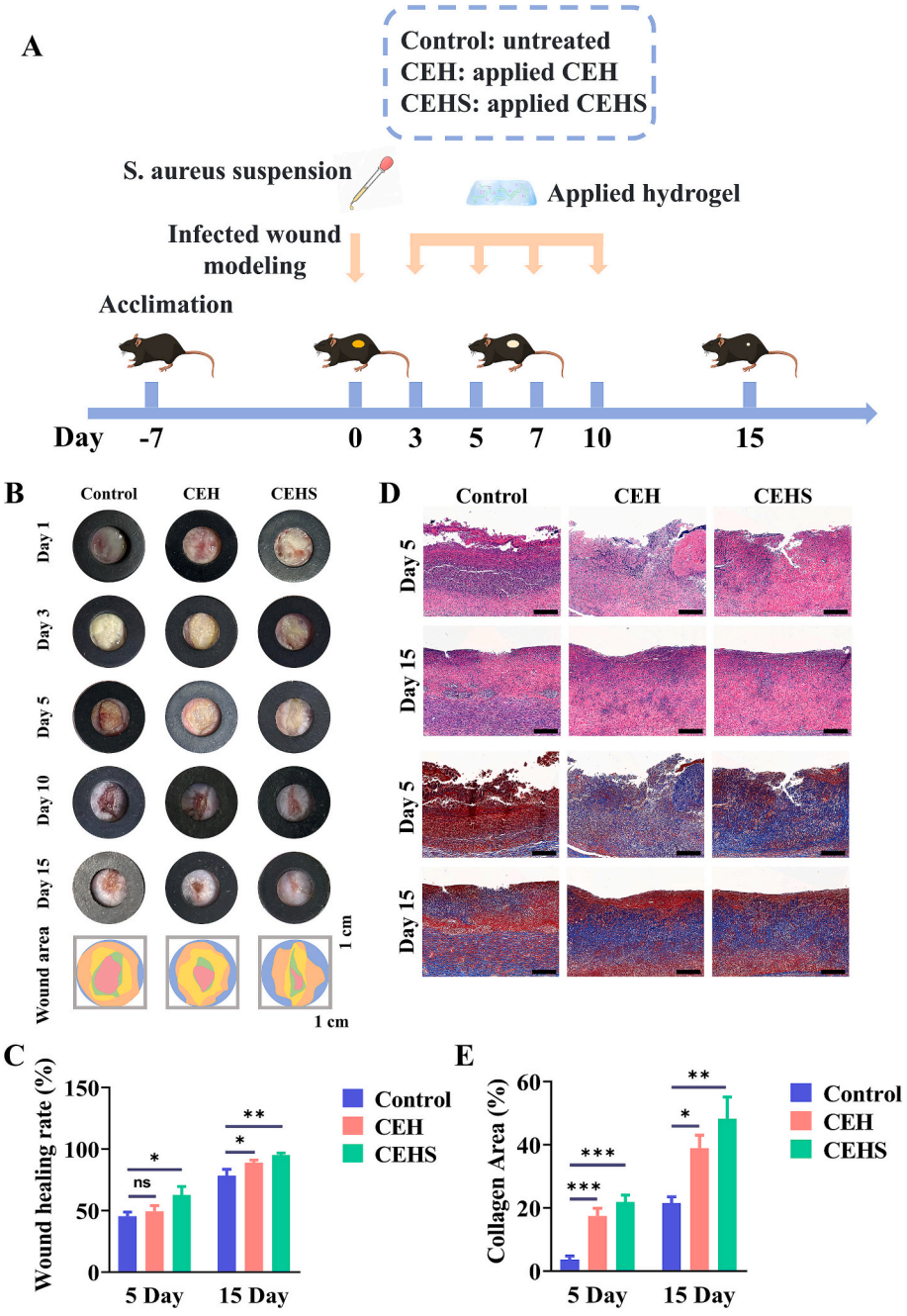

Fig. 5. Evaluation of the therapeutic efficacy of CEHS treatment on infected wounds in mice. (A). Animal experimental procedure for CEHS treatment of infected wounds in mice. (B). The healing status of infected wound images at different time points. (C). Changes in wound healing rates for different groups (n = 3). (D). HE and Masson-stained skin tissue sections of the wound areas from each group on days 5 and 15. Scale bar is 200 μm. (E). Relative collagen content of different groups on days 5 and 15 (n = 3). All data are shown as the mean ± SD. Compared with control group, ns ≥ 0.05, *p < 0.05, **p < 0.01, ***p < 0.001.

role in suppressing early inflammatory responses. Over time, as the wound progressed to the later stages of healing (day 15), inflammatory cell infiltration in both experimental groups decreased further, indicating a successful transition to the proliferative phase. At this stage, the CEH and CEHS groups both showed signs of epithelial tissue regeneration, which were superior to the control group, suggesting smooth cell proliferation and tissue repair processes. Collagen plays a central role in wound healing, with its deposition, remodeling, and metabolism accompanying the healing process. Therefore, the level of collagen deposition reflects the healing status of the wound. Throughout the entire healing period, both the CEH and CEHS groups exhibited higher levels of collagen deposition compared to the control group. By quantitatively analyzing the Masson collagen-positive area, it was evident that the CEHS group had the highest collagen deposition (Fig. 5E). The CEHS group showed a significant increase in collagen-positive area on day 5, and by day 15, collagen staining levels had stabilized with a more dense and regular arrangement of collagen fibers. This indicates that CEHS promotes collagen deposition and fills the wound in the early stages of repair, and in the later stages, it facilitates a dense and regular collagen alignment, ultimately contributing to enhanced tissue mechanical strength, reduced wound space, and complete maturation and functional recovery of the wound.

These results demonstrate that CEHS has excellent potential in promoting the healing of infected wounds. Changes in body weight serve

not only as indirect indicators of metabolic status and the severity of inflammation but also as important parameters for assessing therapeutic efficacy and quality of life (Koh et al., 2005). Therefore, we analyzed the body weight changes in infected mice. The CEHS group showed a relatively slower rate of weight loss compared to the other two groups (Figure S4B). This difference in weight loss further supports the therapeutic effects of CEHS on infected wounds.

3.5. *Antioxidant, anti-inflammatory, antibacterial and pro-vascular effects of CEHS in vivo*

Based on the results of previous cellular experiments, CEHS has demonstrated multiple biological activities, including antioxidant, anti-inflammatory, antibacterial, and pro-angiogenic effects, as well as promoting cell proliferation. In the mouse model of infected wounds, we systematically validated the findings from the in vitro experiments. First, dihydroethidium (DHE) staining was used to assess the degree of oxidative damage in the wounds, where stronger red fluorescence indicates higher levels of oxidative stress. The results showed that compared to day 5, the fluorescence intensity in all groups decreased by day 15, but the fluorescence intensity in the CEH and CEHS groups remained significantly lower than that in the control group (Fig. 6A). This indicates that both CEH and CEHS effectively reduced oxidative stress levels within the wounds. Quantitative analysis of the fluorescence intensity in each group (Fig. 6B) revealed that the CEHS group exhibited the best antioxidant effect. This result not only confirms the superior ability of CEHS to alleviate oxidative damage but also further demonstrates that it effectively neutralizes free radicals and reduces cellular damage, providing a solid foundation for the complete elimination of oxidative stress in infected wounds. Reduced superoxide dismutase (SOD) activity and increased malondialdehyde (MDA) levels typically indicate an imbalance in the cellular oxidative and antioxidant systems, reflecting a weakened in vivo antioxidant defense system. Therefore, we evaluated the in vivo antioxidant activity of CEHS by

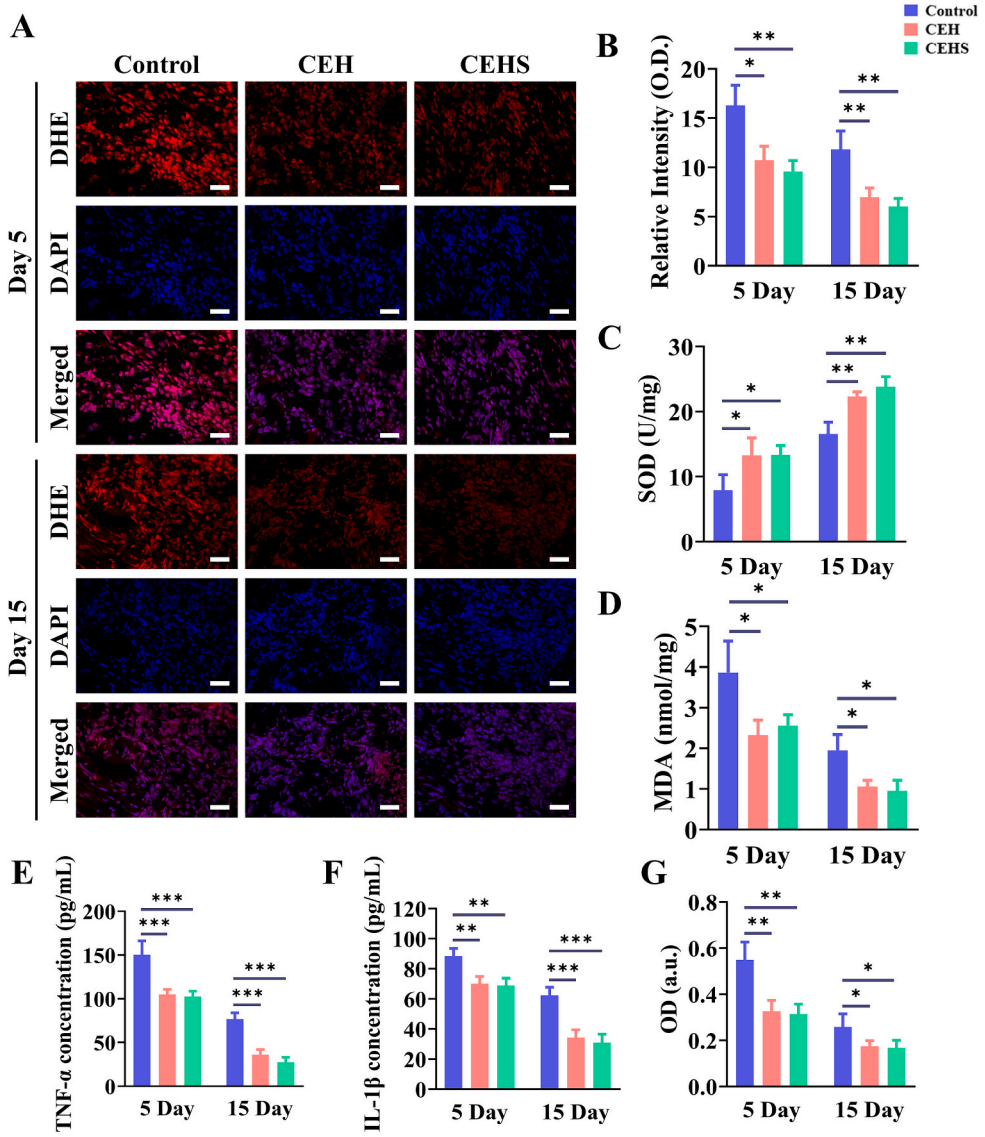

Fig. 6. Antioxidant, anti-inflammatory, and antibacterial activities of CEHS in vivo. (A). Evaluation of oxidative stress of wound tissues by DHE fluorescence staining in different groups on days 5 and 15. Scale bar is 100 μm. (B). Quantitative analysis of the fluorescence intensity of DHE in Fig. (A). The indexes of skin tissues antioxidant were evaluated in different groups. The levels of SOD (C) and MDA (D) changed in different groups on days 5 and 15 (n = 3). The indexes of skin tissue inflammation were evaluated in different groups. The levels of TNF-α (E) and IL-1β (F) changed in different groups on days 5 and 15 (n = 4). (G). Quantitative analysis of wound tissue bacteria in different groups on days 5 and 15 (n = 4). All data are shown as the mean ± SD. Compared with control group, ns ≥ 0.05, *p < 0.05, **p < 0.01, ***p < 0.001.

measuring the SOD activity and MDA levels in the skin tissues of the wounds from each group. Compared to the control group, the CEH and CEHS groups showed significantly increased SOD activity and significantly decreased MDA levels at both day 5 and day 15 (Fig. 6C, D). Based on these experimental results, we can further infer that CEHS enhances SOD activity and reduces MDA levels, thereby mitigating oxidative stress responses and protecting skin cells from free radical damage, which ultimately accelerates the repair and regeneration of the wounds.

To further investigate the anti-inflammatory effects of CEHS in vivo, we used ELISA to measure the levels of TNF-α and IL-1β, two inflammatory cytokines, in the skin tissues of the wounds from each group. The CEH and CEHS groups showed a significant decrease in TNF-α levels compared to the control group, particularly on day 15, where the TNF-α content in the CEHS group was the lowest, differing from the control group by 49.29 ± 6.78 pg/mL (Fig. 6E). This indicates that CEHS can more effectively inhibit the overexpression of TNF-α. Similarly, the levels of IL-1β in all groups showed a similar trend, with the IL-1β levels in the CEHS group being significantly reduced, decreasing by 31.36 ± 7.27 pg/mL compared to the control group (Fig. 6F). These findings further validate the anti-inflammatory effects of CEHS, demonstrating that it can reduce local inflammatory responses in the wound and potentially promote the healing process by inhibiting the expression of TNF-α and IL-1β inflammatory cytokines. Moreover, CEHS had shown preliminary antibacterial activity in vitro. To further evaluate its antibacterial capability in vivo, we extracted tissue fluids from the infected wound tissues of each group of mice, diluted and centrifuged them to prepare bacterial suspensions, and then measured the absorbance at 600 nm using a microplate reader. The results showed that on both day 5

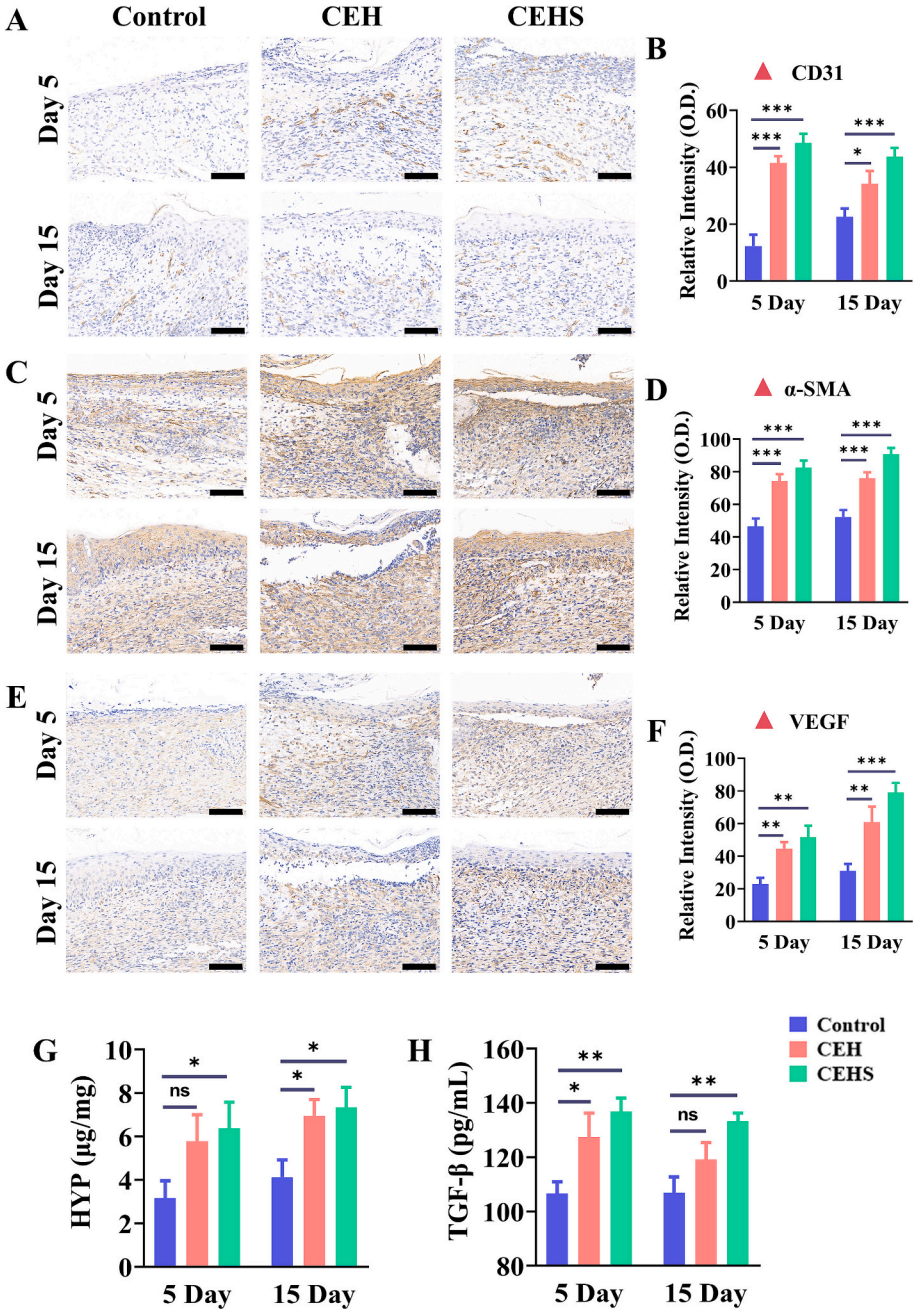

Fig. 7. Analysis of vascularization of CEHS in vivo. Immunohistochemical staining of CD31 (A), α-SMA (C) and VEGF (E) in different groups on days 5 and 15, scale bar = 100 μm. Quantitative analysis of CD31 (B), α-SMA (D) and VEGF (F) positive expression (n = 3). (F). The content of HYP (G) and TGF-β (H) in the wound tissues of each group on days 5 and 15 (n = 3). All data are shown as the mean ± SD. Compared with control group, ns ≥ 0.05, *p < 0.05, **p < 0.01, ***p < 0.001.

and day 15, the absorbance values of the CEH and CEHS groups were significantly lower than those of the control group (Fig. 6G). This indicates that CEHS has significant in vivo antibacterial activity, and CEH also exhibits similar antibacterial properties. These findings suggest that chitosan, a component of the hydrogels, may be the primary agent responsible for the antibacterial effects.

Angiogenesis in wounds plays a critical role in the healing process (Landén et al., 2016). Increased CD31 expression signifies the formation of new blood vessels and endothelial cell activity; monitoring α-SMA helps understand the structure and functional state of the vascular wall; and elevated VEGF levels indicate the activity of angiogenesis and the regulation of related factors. By using these three indicators comprehensively, the state of angiogenesis can be fully assessed. Immunohistochemistry (IHC) was used to detect the expression of CD31, α-SMA, and VEGF in the skin tissues of the wounds, and the results showed that the CEH and CEHS groups exhibited superior CD31, α-SMA, and VEGF positive expression compared to the control group (Fig. 7A, C, E). Further quantitative analysis revealed that the CEHS group had the highest positive expression of CD31, α-SMA, and VEGF (Fig. 7B, D, F). These findings suggest that CEH and CEHS treatments can significantly promote angiogenesis and the maturation of vascular smooth muscle cells during the wound healing process. Notably, CEHS treatment showed a more prominent effect in promoting angiogenesis and vascular function. The expression of α-SMA and VEGF in all groups consistently increased from day 5 to day 15. However, there was a slight decrease in CD31 expression during this period, possibly due to the gradual maturation and stabilization of new blood vessels in the later stages of healing, leading to a reduction in endothelial cell proliferation and migration activities. As a result, CD31 expression also decreased. During this time, the maturation of vascular smooth muscle cells and the expression of angiogenic factors gradually intensified, contributing to the progression of wound healing.

Hydroxyproline (HYP) is a major component of collagen, and elevated levels of HYP indicate enhanced collagen synthesis activity (Cui et al., 2007). In the CEHS group, HYP levels were higher than in the other two groups and reached 7.34 ± 0.92 μg/mg by day 15 (Fig. 7G). These data further confirm that CEHS, by significantly increasing HYP content, enhances collagen synthesis and vascular matrix reconstruction, demonstrating superior efficacy in promoting the formation and reconstruction of new blood vessels. Additionally, transforming growth factor-β (TGF-β) plays a crucial wound healing by promoting angiogenesis (Valluru et al., 2011). The TGF-β content in the wound tissues was measured using ELISA, and the results were consistent with the aforementioned experiments. The CEHS group had the highest TGF-β content, reaching 136.84 ± 4.96 pg/mL on day 5 and slightly decreasing to 133.23 ± 2.98 pg/mL by day 15 (Fig. 7H). In contrast, the TGF-β content in the CEH group and the control group was lower. These results further support the superior performance of the CEHS group in promoting wound healing. The slight decrease in TGF-β levels by day 15 may be due to the wound healing process entering the remodeling phase, where TGF-β shifts its role to help with the restructuring of tissue and the maturation of fibrosis. Moreover, changes in cell signaling and the local microenvironment may also contribute to the decrease in TGF-β concentration.

In summary, the CEHS group not only showed significantly higher expression of CD31, α-SMA, and VEGF compared to the other two groups but also had the highest HYP content and peak TGF-β levels in the early stages of wound healing. The superior angiogenic promotion in the CEHS group, primarily attributed to the addition of sildenafil, which may enhance endothelial cell activity and improve the local microenvironment, significantly contributed to the repair and reconstruction of wound tissues, accelerating the healing process.

Finally, we further validated the safety of CEHS in vivo, primarily through hemolysis assays and tissue compatibility. The hemolysis assay results showed that CEHS does not cause significant hemolysis of red blood cells (Figure S5A), with a hemolysis rate below 5 % (Figure S5B), indicating that it is safe for in vivo use. Additionally, on day 15 after applying CEHS to the wounds in mice, HE staining of major organs (heart, liver, spleen, lungs, and kidneys) confirmed that there were no significant differences in the tissue structure of these organs compared to healthy mice (Figure S5C). This finding indicates that CEHS has good tissue biocompatibility. The safety validations further support the feasibility and effectiveness of CEHS as a treatment strategy for infected wounds.

Overall, CEHS, as a multifunctional novel wound dressing, demonstrates exceptional potential and highlights its promising therapeutic strategy for infected wounds. Despite the encouraging results shown by CEHS, there are several limitations in this study. The experiments were conducted in a mouse model, which may not fully replicate the complexities of human wound healing. The antibacterial activity of CEHS was tested only against *E. coli* and *S. aureus*, and its efficacy against other clinically relevant pathogens has not been explored. Therefore, it may not provide comprehensive and effective antibacterial protection in the treatment of complex wound infections. Furthermore, while the study confirmed the multiple effects of CEHS in promoting infected wound healing, the specific mechanisms underlying its action remain to be further investigated. Future studies will focus on a more in-depth investigation of CEHS to provide a more solid theoretical foundation for its clinical application.

4. Conclusions

In summary, we prepared a hydrogel composed primarily of natural egg white and chitosan, loaded with sildenafil, using a simple method for the treatment of infected wounds. This natural hydrogel exhibits good degradability, swelling properties, and mechanical strength, meeting the basic requirements for wound application. A series of in vitro cell experiments validated that CEHS has excellent biocompatibility, promoting cell migration, proliferation, and endothelial cell vascularization. In the mouse model of infected wounds, CEHS demonstrated therapeutic effects through a combination of antioxidant properties, anti-inflammatory activity, bacterial clearance, and promotion of angiogenesis. Specifically, CEHS effectively reduced oxidative stress, inhibited the overexpression of inflammatory cytokines such as TNF-α and IL-1β, eliminated bacterial infections, and promoted the formation of new blood vessels, thereby enhancing the healing of infected wounds. In conclusion, CEHS offers a promising alternative material for the field of infected wound healing, showcasing significant potential for practical applications.

CRediT authorship contribution statement

Yifan Lai: Writing – original draft, Investigation. **Wa Zhang:** Validation, Formal analysis, Data curation. **Yizhang Chen:** Validation. **Jialu Weng:** Validation, Formal analysis. **Yuhan Zeng:** Validation. **Shunfu Wang:** Visualization, Validation. **Xiaoying Niu:** Formal analysis. **Meilin Yi:** Formal analysis. **Haobing Li:** Formal analysis. **Xuchen Deng:** Validation. **Xiuhua Zhang:** Conceptualization. **Danyun Jia:** Resources, Funding acquisition. **Wenzhang Jin:** Writing – review & editing, Supervision, Methodology, Data curation. **Fajing Yang:** Resources, Funding acquisition, Conceptualization.

Ethics approval statement

All animal procedures in this experiment have been approved by the Ethics Committee of the First Affiliated Hospital of Wenzhou Medical University and the Experimental Animal Management Committee of Zhejiang Province (Approval number.: WYYY-IACUC-AEC-2024-091).

Permission to reproduce material from other sources

No.

Declaration of competing interest

The authors declare no potential conflicts of interest with respect to the research, authorship, and publication of this article.

Acknowledgments

This research was supported by Zhejiang Provincial Natural Science Foundation of China under Grant No. LQ22H290003.

Appendix A. Supplementary data

Supplementary data to this article can be found online at https://doi.org/10.1016/j.ijpx.2025.100328.

Data availability

Data will be made available on request.

References

Abd El-Hack, M.E., El-Saadony, M.T., Shafi, M.E., Zabermawi, N.M., Arif, M., Batiha, G. E., Khafaga, A.F., Abd El-Hakim, Y.M., Al-Sagheer, A.A., 2020. Antimicrobial and antioxidant properties of chitosan and its derivatives and their applications: a review. Int. J. Biol. Macromol. 164, 2726–2744. https://doi.org/10.1016/j.ijbiomac.2020.08.153.

Abrahamian, F.M., Goldstein, E.J., 2011. Microbiology of animal bite wound infections. Clin. Microbiol. Rev. 24, 231–246. https://doi.org/10.1128/cmr.00041-10.

Barros, N.R., Kim, H.-J., Gouidie, M.J., Lee, K., Bandaru, P., Banton, E.A., Sarikhani, E., Sun, W., Zhang, S., Cho, H.-J., 2021. Biofabrication of endothelial cell, dermal fibroblast, and multilayered keratinocyte layers for skin tissue engineering. Biofabrication 13, 035030. https://doi.org/10.1088/1758-5090/aba503.

Bobadilla, A.V.P., Arévalo, J., Sarró, E., Byrne, H.M., Maini, P.K., Carraro, T., Balocco, S., Meseguer, A., Alarcón, T., 2019. In vitro cell migration quantification method for scratch assays. J. R. Soc. Interface 16, 20180709. https://doi.org/10.1098/rsif.2018.0709.

Cai, C., Li, W., Zhang, X., Cheng, B., Chen, S., Zhang, Y., 2024. Natural polymer–based hydrogel dressings for wound healing. Adv. Wound Care. https://doi.org/10.1089/wound.2024.0024.

Castaneda, O.A., Lee, S.-C., Ho, C.-T., Huang, T.-C., 2017. Macrophages in oxidative stress and models to evaluate the antioxidant function of dietary natural compounds. J. Food Drug Anal. 25, 111–118. https://doi.org/10.1016/j.jfda.2016.11.006.

Chang, Q., Darabi, M.A., Liu, Y., He, Y., Zhong, W., Mequanin, K., Li, B., Lu, F., Xing, M. M., 2019. Hydrogels from natural egg white with extraordinary stretchability, direct-writing 3D printability and self-healing for fabrication of electronic sensors and actuators. J. Mater. Chem. A 7, 24626–24640. https://doi.org/10.1039/c9ta06233e.

Chen, Y.-E., Xu, S.-J., Lu, Y.-Y., Chen, S.-X., Du, X.-H., Hou, S.-Z., Huang, H.-Y., Liang, J., 2021. Asperuloside suppressing oxidative stress and inflammation in DSS-induced chronic colitis and RAW 264.7 macrophages via Nrf2/HO-1 and NF-κB pathways. Chem. Biol. Interact. 344, 109512. https://doi.org/10.1016/j.cbi.2021.109512.

Chenani, H., Saeidi, M., Rastkhiz, M.A., Bolghanabadi, N., Aghaii, A.H., Orouji, M., Hatamie, A., Simchi, A., 2024. Challenges and advances of hydrogel-based wearable electrochemical biosensors for real-time monitoring of biofluids: from lab to market. A Review. Analytical Chemistry 96, 8160–8183. https://doi.org/10.1021/acs.analchem.3c03942.

Cheng, S., Pan, M., Hu, D., Han, R., Li, L., Bei, Z., Li, Y., Sun, A., Qian, Z., 2023. Adhesive chitosan-based hydrogel assisted with photothermal antibacterial property to prompt mice infected skin wound healing. Chin. Chem. Lett. 34, 108276. https://doi.org/10.1016/j.cclet.2023.108276.

Chu, W., Wang, P., Ma, Z., Peng, L., Guo, C., Fu, Y., Ding, L., 2023. Lupeol-loaded chitosan-Ag+ nanoparticle/sericin hydrogel accelerates wound healing and effectively inhibits bacterial infection. Int. J. Biol. Macromol. 243, 125310. https://doi.org/10.1016/j.ijbiomac.2023.125310.

Cui, F.-Z., Li, Y., Ge, J., 2007. Self-assembly of mineralized collagen composites. Materials Science and Engineering: R: Reports 57, 1–27. https://doi.org/10.1016/j.mser.2007.04.001.

Ding, J., Xu, K., Xu, H., Ji, J., Qian, Y., Shen, J., 2024. Advances in Gas Therapeutics for Wound Healing: Mechanisms, delivery Materials, and prospects. Small Struct. 5, 2300151. https://doi.org/10.1002/sstr.202300151.

Dong, X., Zhang, Y.Q., 2021. An insight on egg white: from most common functional food to biomaterial application. J. Biomed. Mater. Res. B Appl. Biomater. 109, 1045–1058. https://doi.org/10.1002/jbm.b.34768.

ElHady, A.K., El-Gamil, D.S., Abdel-Halim, M., Abadi, A.H., 2023. Advancements in phosphodiesterase 5 inhibitors: unveiling present and future perspectives. Pharmaceuticals 16, 1266. https://doi.org/10.3390/ph16091266.

Falabella, A.F., 2006. Debridement and wound bed preparation. Dermatol. Ther. 19, 317–325. https://doi.org/10.1111/j.1529-8019.2006.00090.x.

Gao, Y.-M., Li, Z.-Y., Zhang, X.-J., Zhang, J., Li, Q.-F., Zhou, S.-B., 2023. One-pot synthesis of bioadhesive double-network hydrogel patch as disposable wound dressing. ACS Appl. Mater. Interfaces 15, 11496–11506. https://doi.org/10.1021/acsami.2c19931.

Golan, Y., 2019. Current Treatment Options for Acute Skin and Skin-structure Infections. Clin. Infect. Dis. 68, S206–s212. https://doi.org/10.1093/cid/ciz004.

Halcox, J.P., Nour, K.R., Zalos, G., Mincemoyer, R., Waclawiw, M.A., Rivera, C.E., Willie, G., Ellahham, S., Quyyumi, A.A., 2002. The effect of sildenafil on human vascular function, platelet activation, and myocardial ischemia. J. Am. Coll. Cardiol. 40, 1232–1240. https://doi.org/10.1016/s0735-1097(02)02139-3.

Helander, I., Nurmiaho-Lassila, E.-L., Ahvenainen, R., Rhoades, J., Roller, S., 2001. Chitosan disrupts the barrier properties of the outer membrane of Gram-negative bacteria. Int. J. Food Microbiol. 71, 235–244. https://doi.org/10.1016/j.ijbiomac.2020.08.153.

Heunis, T.D., Smith, C., Dicks, L.M., 2013. Evaluation of a nisin-eluting nanofiber scaffold to treat Staphylococcus aureus-induced skin infections in mice. Antimicrob. Agents Chemother. 57, 3928–3935. https://doi.org/10.1016/j.cclet.2023.108276.

Huemer, M., Mairpady Shambat, S., Brugger, S.D., Zinkernagel, A.S., 2020. Antibiotic resistance and persistence—Implications for human health and treatment perspectives. EMBO Rep. 21, e51034. https://doi.org/10.15252/embr.202051034.

Jalili-Firoozinezhad, S., Filippi, M., Mohabatpour, F., Letourneur, D., Scherberich, A., 2020. Chicken egg white: Hatching of a new old biomaterial. Mater. Today 40, 193–214. https://doi.org/10.1016/j.mattod.2020.05.022.

Jin, W., Shen, S., Xu, X., Xie, X., Zhou, X., Su, X., Wu, L., Wang, S., Zhang, L., Chen, B., 2024a. All-in-one hydrogel patches with sprayed bFGF-loaded GelMA microspheres for infected wound healing studies. Int. J. Pharm. 658, 124205. https://doi.org/10.1016/j.ijpharm.2024.124205.

Jin, W., Xie, X., Shen, S., Zhou, X., Wang, S., Zhang, L., Su, X., 2024b. Ultrasmall polyvinylpyrrolidone-modified iridium nanoparticles with antioxidant and anti-inflammatory activity for acute pancreatitis alleviation. J. Biomed. Mater. Res. A 112, 988–1003. https://doi.org/10.1002/jbm.a.37679.

Justin, R., Chen, B., 2014. Characterisation and drug release performance of biodegradable chitosan–graphene oxide nanocomposites. Carbohydr. Polym. 103, 70–80. https://doi.org/10.1016/j.carbpol.2013.12.012.

Kesharwani, P., Bisht, A., Alexander, A., Dave, V., Sharma, S., 2021. Biomedical applications of hydrogels in drug delivery system: an update. Journal of Drug Delivery Science and Technology 66, 102914. https://doi.org/10.1016/j.jddst.2021.102914.

Koh, K.K., Han, S.H., Quon, M.J., 2005. Inflammatory markers and the metabolic syndrome: insights from therapeutic interventions. J. Am. Coll. Cardiol. 46, 1978–1985. https://doi.org/10.1016/j.jacc.2005.06.082.

Kumar, M., Hilles, A.R., Ge, Y., Bhatia, A., Mahmood, S., 2023a. A review on polysaccharides mediated electrospun nanofibers for diabetic wound healing: their current status with regulatory perspective. Int. J. Biol. Macromol. 234, 123696. https://doi.org/10.1016/j.ijbiomac.2023.123696.

Kumar, M., Kumar, D., Garg, Y., Mahmood, S., Chopra, S., Bhatia, A., 2023b. Marine-derived polysaccharides and their therapeutic potential in wound healing application-a review. Int. J. Biol. Macromol. 253, 127331. https://doi.org/10.1016/j.ijbiomac.2023.127331.

Kumar, M., Kumar, D., Kumar, D., Garg, Y., Chopra, S., Bhatia, A., 2024. Therapeutic potential of Nanocarrier Mediated delivery of Peptides for Wound Healing: Current Status. Challenges and Future Prospective. AAPS PharmSciTech 25, 108. https://doi.org/10.1208/s12249-024-02827-5.

Landén, N.X., Li, D., Ståhle, M., 2016. Transition from inflammation to proliferation: a critical step during wound healing. Cell. Mol. Life Sci. 73, 3861–3885. https://doi.org/10.1007/s00018-016-2268-0.

Li, L., Low, M.-Y., Ge, X., Bloodworth, B.C., Koh, H.-L., 2009. Isolation and structural elucidation of dapoxetine as an adulterant in a health supplement used for sexual performance enhancement. J. Pharm. Biomed. Anal. 50, 724–728. https://doi.org/10.1016/j.jpba.2009.06.005.

Li, Y., Nie, L., Jin, S., Sun, C., Lu, X., 2022. The effect of Plasma on Bacteria and Normal Cells in Infected Wound. Oxid. Med. Cell. Longev. 2022, 1838202. https://doi.org/10.1155/2022/1838202.

Liang, Y., He, J., Guo, B., 2021. Functional hydrogels as wound dressing to enhance wound healing. ACS Nano 15, 12687–12722. https://doi.org/10.1021/acsnano.1c04206.

Liu, H., Wang, C., Li, C., Qin, Y., Wang, Z., Yang, F., Li, Z., Wang, J., 2018. A functional chitosan-based hydrogel as a wound dressing and drug delivery system in the treatment of wound healing. RSC Adv. 8, 7533–7549. https://doi.org/10.1039/c7ra13510f.

Ma, J., Li, G., Wang, H., Mo, C., 2024. Comprehensive review of potential drugs with anti-pulmonary fibrosis properties. Biomed. Pharmacother. 173, 116282. https://doi.org/10.1016/j.biopha.2024.116282.

Mamun, A.A., Shao, C., Geng, P., Wang, S., Xiao, J., 2024. Recent advances in molecular mechanisms of skin wound healing and its treatments. Front. Immunol. 15, 1395479. https://doi.org/10.3389/fimmu.2024.1395479.

Mo, F., Zhang, M., Duan, X., Lin, C., Sun, D., You, T., 2022. Recent advances in Nanozymes for Bacteria-Infected Wound Therapy. Int. J. Nanomedicine 17, 5947–5990. https://doi.org/10.2147/ijn.S382796.

Naahidi, S., Jafari, M., Logan, M., Wang, Y., Yuan, Y., Bae, H., Dixon, B., Chen, P., 2017. Biocompatibility of hydrogel-based scaffolds for tissue engineering applications. Biotechnol. Adv. 35, 530–544. https://doi.org/10.1016/j.biotechadv.2017.05.006.

Ng, V.W., Chan, J.M., Sardon, H., Ono, R.J., García, J.M., Yang, Y.Y., Hedrick, J.L., 2014. Antimicrobial hydrogels: a new weapon in the arsenal against multidrug-resistant infections. Adv. Drug Deliv. Rev. 78, 46–62. https://doi.org/10.1016/j.addr.2014.10.028.

Qiao, J., Jiang, Y., Ren, Z., Tang, K., 2023. Protocatechualdehyde-ferric iron tricomplex embedded gelatin hydrogel with adhesive, antioxidant and photothermal

antibacterial capacities for infected wound healing promotion. Int. J. Biol. Macromol. 242, 125029. https://doi.org/10.1016/j.ijbiomac.2023.125029.
Rafati, Z., Sirousazar, M., Hassan, Z.M., Kheiri, F., 2020. Honey-loaded egg white/poly (vinyl alcohol)/clay bionanocomposite hydrogel wound dressings: in vitro and in vivo evaluations. J. Polym. Environ. 28, 32–46. https://doi.org/10.1007/s10924-019-01586-w.
Santoro, A., Martucci, M., Conte, M., Capri, M., Franceschi, C., Salvioli, S., 2020. Inflammaging, hormesis and the rationale for anti-aging strategies. Ageing Res. Rev. 64, 101142. https://doi.org/10.1016/j.arr.2020.101142.
Shrestha, S., Shrestha, B.K., Tettey-Engmann, F., Auniq, R.B.Z., Subedi, K., Ghimire, S., Desai, S., Bhattarai, N., 2024. Zein-coated Zn metal particles-incorporated nanofibers: a potent fibrous platform for loading and release of Zn ions for wound healing application. ACS Appl. Mater. Interfaces 16, 49197–49217. https://doi.org/10.1021/acsami.4c13458.
Su, G., Xu, H., Marrone, G., Lindholm, B., Wen, Z., Liu, X., Carrero, J.J., Lundborg, C.S., 2017. Chronic kidney disease is associated with poorer in-hospital outcomes in patients hospitalized with infections: Electronic record analysis from China. Sci. Rep. 7, 11530. https://doi.org/10.1038/s41598-017-11861-2.
Tonnesen, M.G., Feng, X., Clark, R.A., 2000. Angiogenesis in wound healing. In: Journal of investigative dermatology symposium proceedings. Elsevier, pp. 40–46. https://doi.org/10.1016/0163-7258(91)90034-j.
Unterman, S., Charles, L.F., Strecker, S.E., Kramarenko, D., Pivovarchik, D., Edelman, E. R., Artzi, N., 2017. Hydrogel nanocomposites with independently tunable rheology and mechanics. ACS Nano 11, 2598–2610. https://doi.org/10.1021/acsnano.6b06730.
Valluru, M., Staton, C.A., Reed, M.W., Brown, N.J., 2011. Transforming growth factor-β and endoglin signaling orchestrate wound healing. Front. Physiol. 2, 89. https://doi.org/10.3389/fphys.2011.00089.
Wang, X., Ma, Y., Niu, X., Su, T., Huang, X., Lu, F., Chang, Q., 2022. Direct three-dimensional printed egg white hydrogel wound dressing promotes wound healing with hitching adipose stem cells. Front. Bioeng. Biotechnol. 10, 930551. https://doi.org/10.1016/j.cclet.2023.108276.
Webster, J., Scuffham, P., Stankiewicz, M., Chaboyer, W.P., 2014. Negative pressure wound therapy for skin grafts and surgical wounds healing by primary intention. The Cochrane database of systematic reviews Cd009261. https://doi.org/10.1002/14651858.CD009261.pub3.
Wilkinson, H.N., Hardman, M.J., 2020. Wound healing: cellular mechanisms and pathological outcomes. Open Biol. 10, 200223. https://doi.org/10.1098/rsob.200223.
Xiao, N., Huang, X., He, W., Yao, Y., Wu, N., Xu, M., Du, H., Zhao, Y., Tu, Y., 2021. A review on recent advances of egg byproducts: Preparation, functional properties, biological activities and food applications. Food Res. Int. 147, 110563. https://doi.org/10.1016/j.foodres.2021.110563.
Yang, F., Qiu, Y., Xie, X., Zhou, X., Wang, S., Weng, J., Wu, L., Ma, Y., Wang, Z., Jin, W., 2024. Platelet Membrane-Encapsulated Poly (lactic-co-glycolic acid) Nanoparticles Loaded with Sildenafil for Targeted Therapy of Vein Graft Intimal Hyperplasia. International Journal of Pharmaceutics: X 8, 100278. https://doi.org/10.1016/j.ijpx.2024.100278.
Zhang, H., Lin, X., Cao, X., Wang, Y., Wang, J., Zhao, Y., 2024a. Developing natural polymers for skin wound healing. Bioactive Materials 33, 355–376. https://doi.org/10.1016/j.bioactmat.2023.11.012.
Zhang, J., Zhao, S., Zhou, Y., Liang, H., Zhao, L., Tan, H., 2024b. Carboxymethyl Chitosan-based Antioxidant Hydrogel Accelerates Diabetic Wound Healing. Adv. Healthc. Mater. 2403198. https://doi.org/10.1002/adhm.202403198.